Impure Carbon Nanotubes as Reinforcements for Acrylated Epoxidized Soy Oil Composites

Wim Thielemans,[1*] Ian M. McAninch,[1] Valerie Barron,[2] Werner J. Blau,[2] Richard P. Wool[1]

[1]*Department of Chemical Engineering and Center for Composite Materials, University of Delaware, Newark, Delaware 19716*
[2]*Department of Physics, Trinity College Dublin, Dublin 2, Ireland*

Received 13 September 2004; accepted 3 March 2005
DOI 10.1002/app.22372
Published online in Wiley InterScience (www.interscience.wiley.com).

ABSTRACT: Stable dispersions of impure multiwall carbon nanotubes (multiwall carbon nanotubes and carbon soot) in an acrylated epoxidized soy oil (AESO) based thermosetting resin were obtained by mechanical stirring. The required stirring time increased with an increasing amount of carbon nanotubes. Thermogravimetric analysis of the polymerized samples showed some loss of multiwall carbon nanotubes due to sedimentation. The mechanical properties of the polymerized samples improved significantly (the modulus increased by 30%) for 0.28 wt % dispersed multiwall carbon nanotubes. Higher multiwall carbon nanotube loads resulted in significant aggregation during polymerization. The mechanical properties were compared with existing models for nanocomposites. Wide-angle X-ray scattering, optical microscopy, and transmission electron microscopy demonstrated the formation of aggregates at higher multiwall carbon nanotube loads, which reversed the potential for mechanical improvement. Because of the stability of the original dispersion, the aggregates were believed to form during polymerization. This aggregation was magnified by the carbon soot, so only small amounts of impure multiwall carbon nanotubes could be used as reinforcements. Transmission electron micrographs showed good adhesion of the polymer matrix to the nanotubes upon the rupture of the polymer matrix. AESO was believed to act as a solubilizing surfactant, in line with previously published results. © 2005 Wiley Periodicals, Inc. J Appl Polym Sci 98: 1325–1338, 2005

Key words: composites; dispersions; nanocomposites

INTRODUCTION

Carbon nanotubes (CNTs) have been studied extensively because of their unique mechanical,[1,2] optical,[3,4] electronic,[5,6] and gas storage[7] properties. Their high Young's modulus (~1TPa) and aspect ratio (10–1000) make them ideally suited as reinforcements.[8,9] For the full exploitation of these extraordinary properties, the CNTs have to form stable dispersions.[10] Dispersions have been obtained with a variety of solvents,[11,12] surfactants,[13,14] conjugated polymers,[15–17] sugars,[18–20] and biological molecules[21,22] and by the chemical functionalization of the CNT surface. Chemical functionalization, involving the addition of acid functionality,[23,24] silica,[25] fluorine,[26,27] and alkanes,[28] has the inherent effect of altering the properties of the CNTs by altering the sp^2 hybridization of the carbon atoms and thus the CNT properties.[29] Therefore, benign means of dispersing nanotubes are desired. Richard et al.[30] showed the appearance of a self-assembled structure on the surface of CNTs by synthetic lipids.

Biobased resins have already been used to makes composites with natural fibers, lignin, and glass fibers.[31–36] These resins are based on modified soy oil (Fig. 1) with styrene as a reactive diluent and have proven to be comparable to commercial, petroleum-based thermosetting resins.[31,35] Each fatty acid is about 18 carbons long with 0–3 double bonds per fatty acid arm.[37] The free radically unreactive double bonds of the soy oil are functionalized with acrylate functional groups, which allow free-radical polymerization with a reaction pathway that includes an epoxidation, followed by an acrylation reaction, as shown in Figure 2. The soy oil is made of triglyceride molecules, with three fatty acids joined at a glycerol juncture. This chemical structure, with local polar centers, is similar to synthetic lipids used by Richard et al.[30] It can therefore be assumed that natural oil tryglicerides will have a favorable effect on the dispersion of CNTs. Recently published work has shown that acrylated epoxidized soy oil (AESO) can be used to disperse single-walled carbon nanotubes (SWNTs) in toluene and styrene.[38]

The purpose of this work is to investigate the potential for obtaining a stable dispersion of impure multiwall carbon nanotube (MWNT) powder, obtained from an arc-discharge reactor, in an unsatur-

Correspondence to: R. P. Wool (wool@ccm.udel.edu).
**Present address:* Ecole Française de Papeterie et des Industries Graphiques, BP 65, 38402 Saint-Martin d'Hères, France.
Contract grant sponsor: U.S. Department of Energy.
Contract grant sponsor: U.S. Environmental Protection Agency.

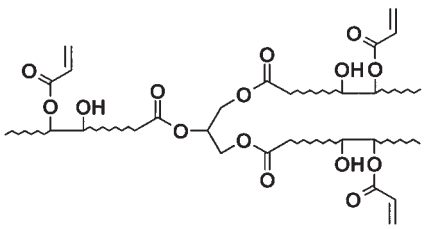

Figure 1 Chemical structure of AESO.

ated triglyceride-based thermosetting resin. Simple mixing has already been successful in dispersing MWNTs in epoxies.[39] This resin is subsequently free-radically polymerized, and the resulting composite is further tested and analyzed. The use of unpurified CNTs, which contain a significant amount of carbon soot, may allow for a cheaper method to form nanocomposites because of the absence of a necessary purification step.

EXPERIMENTAL

Materials

AESO (trade name Ebecryl 860) and styrene (99% pure) were obtained from UCB Chemicals (Brussels, Belgium) and Aldrich Chemicals (St. Louis, MO), respectively. AESO contains on average 3.4 acrylates per triglyceride molecule and acts as a crosslinker during polymerization. *tert*-Butyl peroxybenzoate (98% pure; Aldrich Chemicals) was used as a free-radical initiator.

The MWNTs were prepared with the arc-discharge Krätschmer–Huffman process at Trinity College Dublin (Dublin, Ireland).[40] The crude powder had a nanotube concentration of 30–40%. The remaining 60–70% was carbon soot containing largely pyrolytic carbon and some other carbon nanoparticles. For consistent nomenclature, *carbon soot* denotes the 60–70% non-nanotube carbon and graphitic particles, whereas *MWNT* refers only to the 30–40% MWNTs in the crude powder. A scanning electron microscopy (SEM) micrograph of the crude powder is shown in Figure 3. The micrograph was taken on a JEOL 7400F field emission scanning electron microscope with an acceleration voltage of 1.0 kV. This powder was used as received without any purification steps. The MWNTs in the powder had an average diameter of 24 nm and a length of 800 nm, which resulted in an aspect ratio of 33.3. These dimensions were confirmed by high-resolution SEM and transmission electron microscopy (TEM).

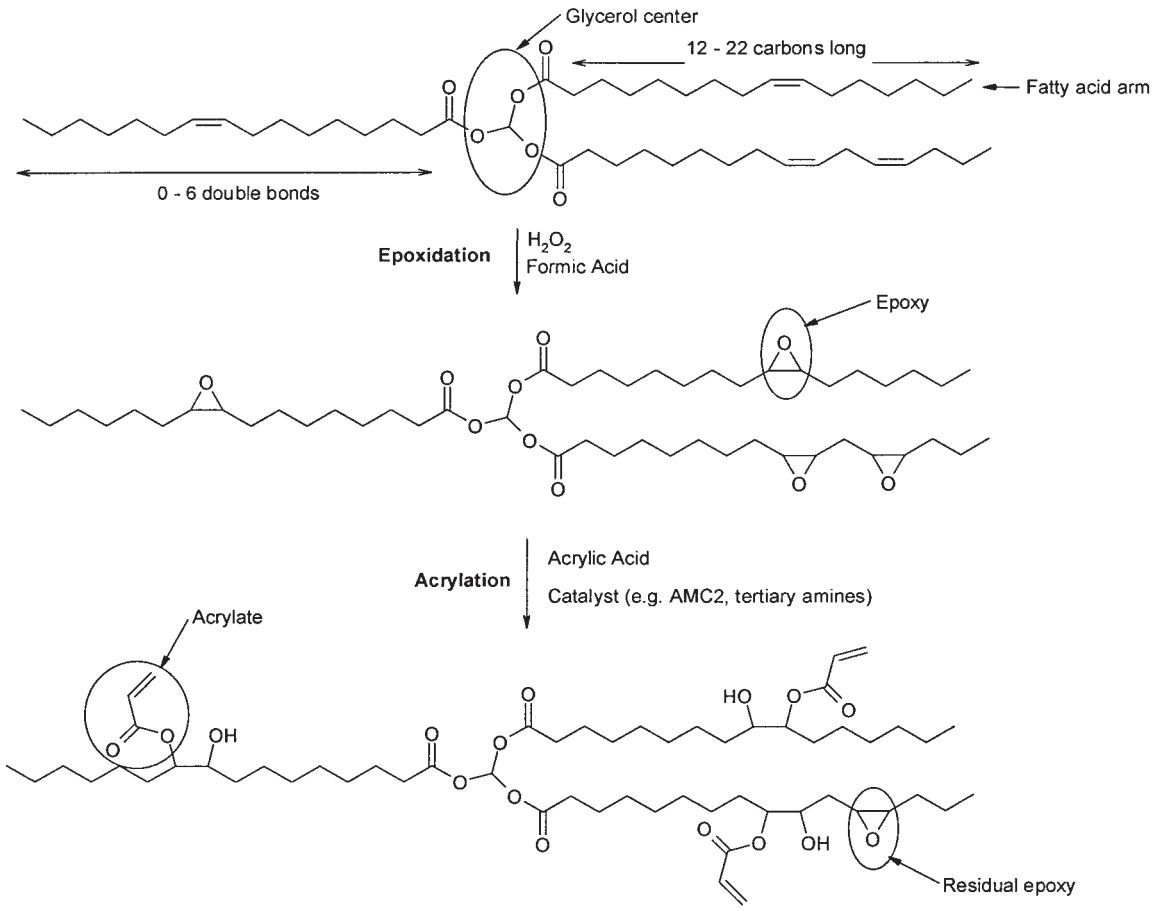

Figure 2 Chemical structure of the triglycerides found in soy oil and the chemical pathway for obtainingAESO.[31]

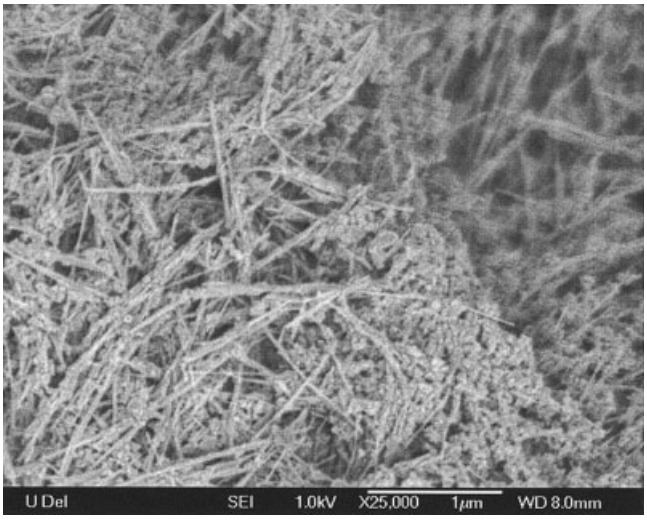

Figure 3 SEM micrograph of the MWNT/carbon soot mixture obtained by the arc discharge used in this work. The MWNT concentration was approximately 65%.

Dispersion

AESO and styrene were mixed in a 65/35 weight ratio. The crude carbon powder and AESO/styrene mixture were added to 20-mL glass vials to obtain 1, 3, and 5 wt % crude powders in the AESO/styrene mixture. The total sample weight was approximately 7.5 g. They were mixed for various amounts of time at 1150 rpm. The 1 wt % sample was stirred for 24 h and then left to settle for 24 h. Sedimentation started to occur after 24 h, so it was stirred again for 24 h, after which it was left to settle again for 24 h. No sedimentation was seen afterwards. The 3 and 5 wt % samples were initially stirred for 48 h and left to settle for 24 h. Only the 5 wt % sample showed signs of sedimentation and was stirred for an additional 24 h. No sedimentation was seen after 24 h of settling. All samples were left to settle for an additional week without visible sedimentation. The dispersion thus appeared to be stable.

Composite preparation

To the stable dispersions, 1.5 wt % *tert*-butyl peroxy benzoate was added, and this was followed by a purging step of the monomer mixture with nitrogen for 2 min to remove all free oxygen. The mixtures were then polymerized in a silicone mold at 110°C for 2 h. The cured samples were postcured at 160°C for an additional 2 h before demolding. Two pure AESO/styrene samples were also prepared and cured at the same time as the dispersion samples. The samples were then polished to a specimen size of approximately 55 × 10 × 5 mm. The 3 wt % sample size was smaller at 35 × 10 × 5 mm because of cracking at one end of the sample during polymerization. No cracks were seen in the sample with an optical microscope. A small section was cut from each composite sample before the polishing for thermogravimetric analysis (TGA).

Measurement

TGA under an active airflow was carried out on a PerkinElmer Pyris 1 TGA instrument (Boston, MA) with a 10 mL/min airflow and a sample weight of approximately 3 mg. The temperature was ramped from 100 to 900°C at a rate of 20°C/min.

The composite sample dynamic mechanical analysis (DMA) was performed on a TA Instruments DMA 2980 (New Castle, DE) in the dual-cantilever mode. The samples were clamped on both ends and deformed in the middle, where the sample was clamped as well. This setup resulted in more stable data than the three-point-bending setup in the region past the glass-transition temperature. However, absolute modulus values depend on the clamping pressure. So that the results could be compared, the sample thickness was constant for all samples, as well as the clamping pressure, which was kept constant with a torque wrench. The testing frequency was 1 Hz, and the temperature was ramped between 30 and 200°C at 2°C/min. The deformation amplitude was 15 μm.

Optical microscopy was carried out on a Leitz compound optical microscope (Leica Microsystems, Bannockburn, IL). The samples were cut from the original DMA samples with a glass knife to a thickness of about 7.5 μm. TEM samples 80 nm thick were obtained by the microtoming of sections at room temperature from the tested DMA samples. The sections were placed on a 400-mesh hexagonal copper grid. TEM was carried out on JEOL 2000FX and 2010F transmission electron microscopes. The acceleration voltage used with both electron microscopes was 200 kV.

Wide-angle X-ray scattering (WAXS) was performed with a Rigaku copper rotating-anode X-ray source (The Woodlands, TX) (Cu Kα, wavelength = 1.54 Å) with a Bruker two-dimensional gas-filled area detector (Madison, WI). The incident beam passed through approximately 5 mm of the composite/polymer sample, which was cut from the used DMA sample and used without additional treatment. The WAXS experiments were run at room temperature for 4 h. The crude powder was tested in a quartz capillary tube for only 1 h because of the much higher signal obtained.

RESULTS AND DISCUSSION

TGA

TGA was used to determine the exact amount of crude powder in the composite samples. The TGA data obtained under an air atmosphere for all samples are combined in Figure 4. The decomposition of the pure polymer starts around 250°C. The maximum rate of

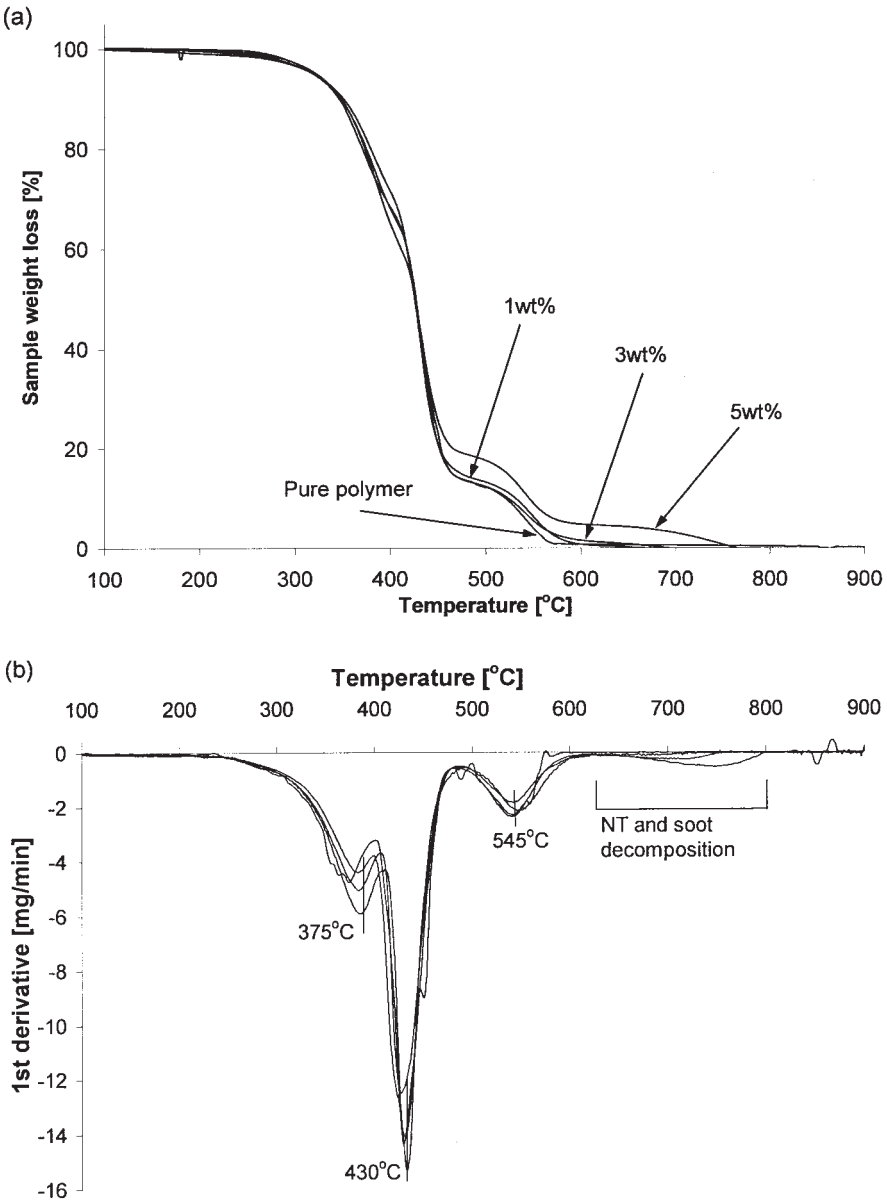

Figure 4 TGA data for the pure polymer and composite samples under an air atmosphere: (a) decomposition data and (b) first derivatives. The plot labels refer to the amount of crude powder (MWNTs and carbon soot) in the original dispersion.

decomposition is reached at 430°C, whereas a local maximum at 375°C can be observed as a small dip in the decomposition profile. An extra shoulder around 545°C can also be seen for the pure polymer sample. This decomposition behavior is similar to the results found for the thermal decomposition of styrene-containing commercial polyesters.[41] The first decomposition at 375°C is attributed to the rupture of crosslinks and the formation of linear chains,[42] the second and largest weight-loss region, around 430°C, is due to random scission of the linear chains into smaller fragments,[42] whereas the high-temperature decomposition at 545°C is characteristic for the complete decomposition of the polyester chain.[41]

The thermal decomposition of the composite samples is largely unchanged from the pure polymer sample, except that the crude powder decomposition appears as a large shoulder between 600 and 800°C. Little change is seen in the positions of the decomposition regions for the polymer matrix. The thermal decomposition of the polymer ends before the decomposition of the crude powder starts. This allows us to calculate the amount of MWNT and carbon soot (total crude powder) in the sample by the relative area under the crude powder first-derivative peak and the first-derivative polymer peaks.[43] The absolute differences in the peak heights shown in Figure 4(b) are due to differences in the initial sample weight and are not due to differences in the decomposition behavior. TGA does not allow a distinction between MWNTs and carbon soot as both decompose over the same temperature range.

TABLE I
Comparison of the Amounts of MWNTs Added to the Monomer Mixture and in the Composite After Sedimentation and Polymerization as Determined by TGA Under and Air Atmosphere.

Initial nominal amount of crude powder (wt %)	Crude powder in the composite (wt %)
1	0.2[a]
3	1.8
5	4.4

[a] Deemed inaccurate because of the small amount of the crude powder.

One can thus obtain only the amount of crude powder in the composite sample.

The TGA results are combined in Table I. The total amount of MWNTs and carbon soot found for the 1 wt % sample was deemed inaccurate because of the small amount of crude powder in the sample. The calculated crude powder fractions show a significantly lower content in the composite than in the original monomer dispersion. This can only be due to sedimentation of either nanotubes or carbon soot particles, even though no apparent sedimentation occurred from the liquid dispersions. The TGA data also show a significant amount of crude powder that was lost in the 3 wt % sample. That could be an indication of a dispersion that was less stable than previously assumed, so sedimentation did occur either during the settling time or the polymerization stage (before gelation).

Mechanical properties

The storage modulus (E') and loss modulus (E'') for the various samples are shown in Figure 5. E' at 35°C, as well as the maxima in E'' and tan δ, are combined in Table II. A significant and comparable increase in E' can be seen for the 1 and 5 wt % samples, whereas the 3 wt % sample does not show any increase in comparison with the pure polymer samples. The most considerable increases in maximum E'' and maximum tan δ can also be seen for the 1 wt % sample. This is a clear indication that the polymer chains in this sample are the most restricted in their movement. This can only be due to dispersed MWNTs. The absence of a change in the modulus for 3 wt % points toward the complete aggregation of carbon soot particles and MWNTs. It has been shown that the addition of a carbon filler does not affect the modulus of thermosetting polymers.[44] On the other hand, a carbon filler is expected to increase the glass-transition temperature,[45] as is seen in the increase in the maxima of E'' and tan δ. It thus appears that all crude powder (MWNTs and carbon soot) is aggregated in the 1.8 wt % composite sample, whereas some MWNTs are dispersed in the other composite samples. This apparent aggregation is also in agreement with the TGA data, in which a loss of 1.2% of the initial crude powder amount was recorded for the 3 wt % dispersion sample. Because this loss can only be due to sedimentation, which is preceded by aggregation, the aggregation of most, if not all, added MWNTs and carbon soot could be expected. The small loss of crude powder for the original 5 wt % solution, determined by TGA, points toward a good original dispersion. It has, however, been shown that carbon black has a tendency to aggregate in clusters during free-radical polymerization.[46] Aggregation has also been shown to occur during the dynamic compounding and processing of thermoplastic polymer melts.[47] It is also well known that carbon black reduces the polymerization rate of *tert*-butyl peroxy benzoate initiated free-radical polymerization.[48] The slower polymerization and higher agglomeration rate for the 5 wt % crude powder dispersion, both due to the higher concentration of carbon soot, result in a significantly larger amount of cluster formation, in comparison with the 1 wt % sample. The apparent result is the encapsulation of a large amount of MWNTs in these aggregates, so they do not contribute to reinforcement. This effect appears to be significant enough to result in a reduced mechanical improvement in comparison with the 1 wt % composite sample. So even when the polymerization is initiated from an initially well-dispersed sample, aggregation is expected and will strongly affect the mechanical properties of the obtained composite sample.

All the composite samples show an increase in the rubber plateau modulus above the glass-transition temperature. A similar rubbery plateau for 1 and 5 wt % MWNT composite samples points to a similar amount of dispersed nanotubes, which is also seen in a similar low-temperature E' value. The additional nanotubes in the 5 wt % sample, determined by TGA where 4.4 wt % crude powder was in the composite sample, were thus expected to be aggregated.

The E'' values for the 1 and 5 wt % MWNT composites [Fig. 5(b)] behave similarly below the glass-transition temperature. In the rubbery regime (above the glass-transition temperature), the ratio of E'' to E', which equals tan δ, for the various composite samples is related as follows:

$$\left(\frac{E''}{E'}\right)_{5\text{wt\%}} > \left(\frac{E''}{E'}\right)_{1\text{ wt\%}} > \left(\frac{E''}{E'}\right)_{3\text{ wt\%}} > \left(\frac{E''}{E'}\right)_{\text{pure resin}} \quad (1)$$

Aggregates thus increase this ratio slightly, whereas dispersed MWNTs have a more pronounced effect on tan δ (following the relations between 5, 1, and 3 wt % samples).

Optical microscopy

Pictures taken with the optical microscope show an increase in the number of black regions as the crude

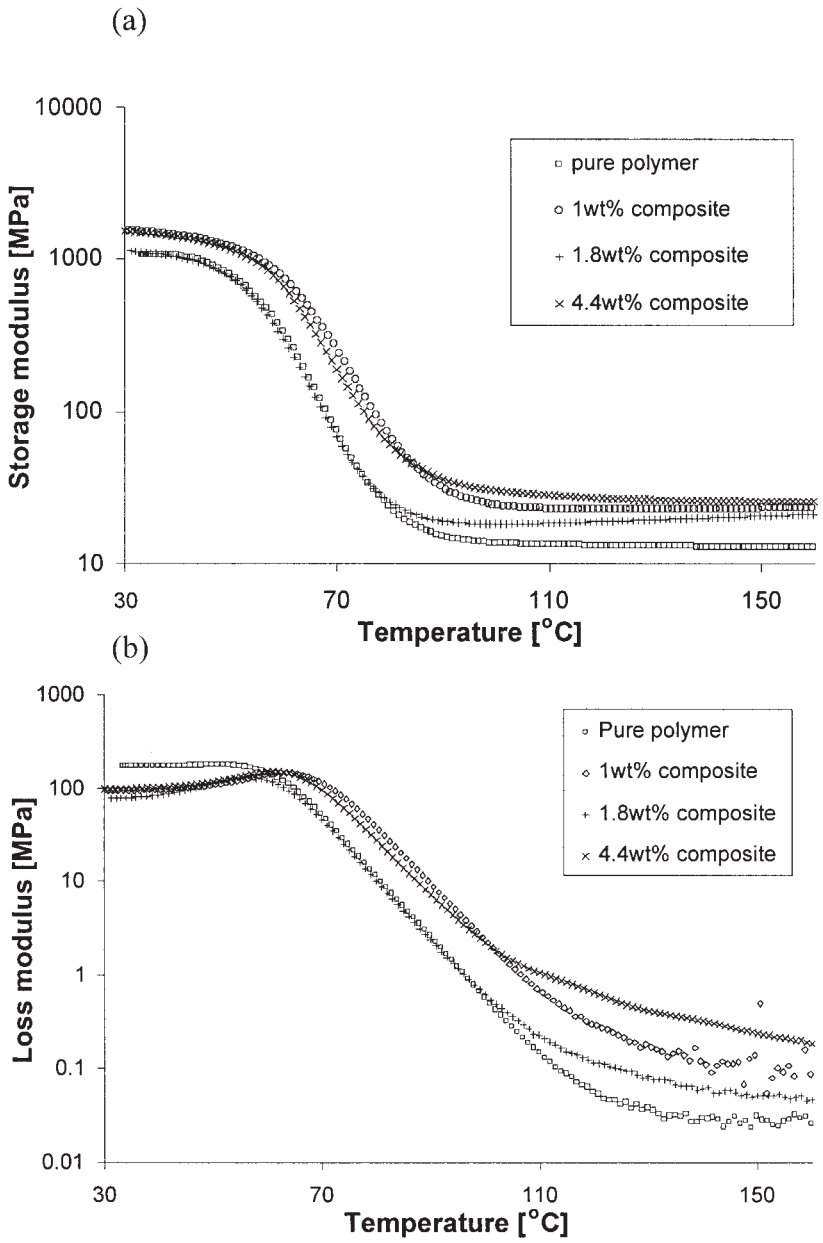

Figure 5 (a) E' and (b) E'' of AESO/styrene (65/35 w/w) composites with various crude powder (MWNTs and carbon soot) concentrations as measured by DMA in the cantilever mode. The crude powder concentrations were obtained from TGA (except for 1 wt %).

powder content increases (Fig. 6). The size of these regions increases with increasing crude powder content as well. These regions are believed to be aggregates of MWNTs and carbon soot. The original size of the dark regions (at 1 wt % MWNT) is between 1 and 5 μm. As the amount of MWNT increases to 4.4 wt %,

TABLE II
Compilation of Important DMA Data for the Different Composite Samples

Crude powder in the solution (wt %)	Crude powder in the composite (wt %)	E' at 35°C (MPa)	Maximum E″ (°C)	Maximum tan δ (°C)
0	0	1.113 ± 0.073	53.4 ± 3.7	70.9 ± 0.5
1	1	1.516	63.8	77.3
3	1.8	1.090	56.7	72.1
5	4.4	1.482	61.5	73.7

The variation for the pure polymer sample is the standard deviation between the two polymer samples.

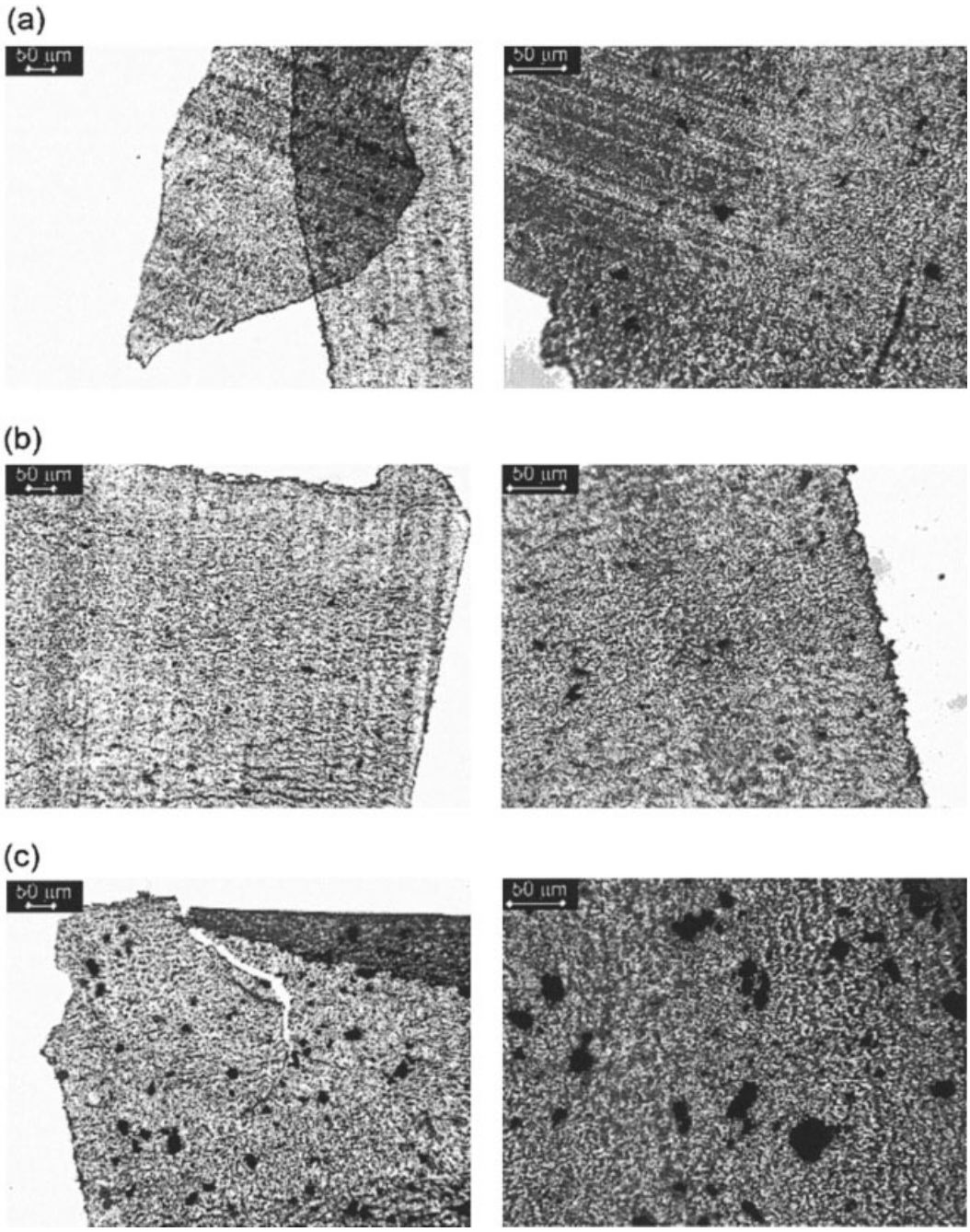

Figure 6 Optical microscopy pictures of various composite samples: (a) 1 wt % composite sample, (b) 1.8 wt % composite sample (3 wt % crude powder in the dispersion), and (c) 4.4 wt % composite sample (5 wt % crude powder in the dispersion).

the size of these regions increases to a range of 10–30 μm.

TEM

The TEM micrographs of a 1 wt % MWNT composite show a very good dispersion of the MWNTs (Fig. 7). Several MWNTs can be found together and aligned. Strong van der Waals forces hold them together, and they cannot be easily broken apart by the shear forces of stirring. Aggregates consist largely of graphitic particles (carbon soot) and contain a very limited amount of MWNTs. Their size is around 1 μm, in agreement with optical microscopy. The significant amount of dispersed MWNTs, whether or not in sets of two aligned tubes, explains the significant improvement in E'. The dispersed MWNTs will act as reinforcements, whereas the MWNTs found in the aggregates are not expected to contribute.

The micrographs of the 4.4 wt % composite samples show large clusters of aggregates (Fig. 8). A large fraction of the clusters is made up of MWNTs. There

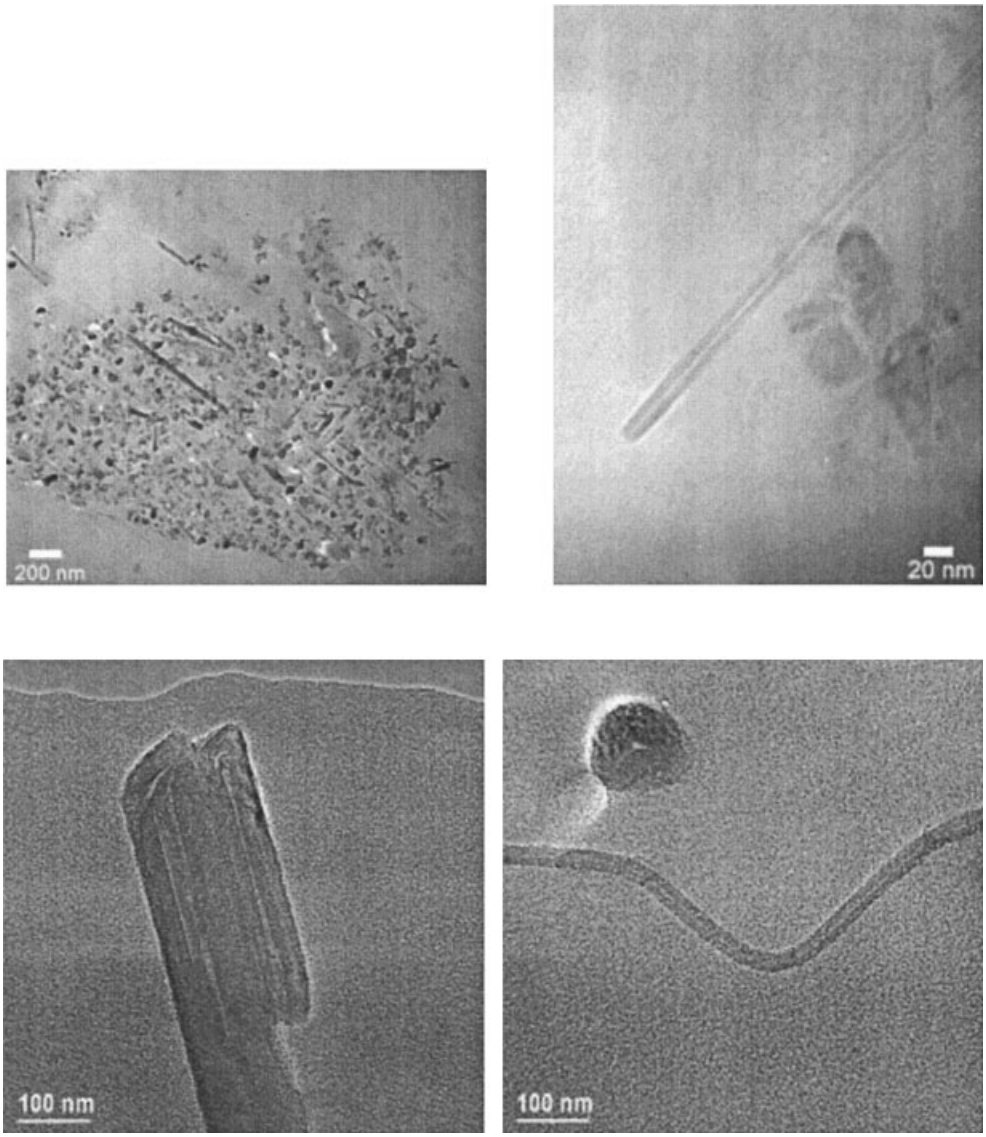

Figure 7 TEM micrographs of the 1 wt % composite sample.

are also a significant number of dispersed nanotubes. These dispersed nanotubes would explain the improved properties, in comparison with the pure polymer samples. The similar improvements of the 1 and 4.4 wt % composite samples point toward a similar amounts of dispersed nanotubes. This is seen in the larger MWNT fraction in the aggregates. Micrographs for the 1.8 wt % composite did not show any significant amount of dispersed MWNTs.

Figure 9 shows TEM micrographs of ruptured sections of the composite samples. The sections were ruptured during microtoming. One can clearly see the polymer sticking to the nanotube when the polymer matrix was pulled apart, and this indicates a strong interface between the polymer matrix and the dispersed nanotubes. The strong interface may be partially due to grafting during the polymerization reaction. A strong interface is paramount for mechanical improvement. The crosslinking of the polymer, however, limits the deformation that the matrix can attain, so the CNT does not stay completely covered by the polymer during composite rupture. If grafting does occur, it is thus limited, or the whole surface of the nanotubes would be expected to stay covered. A large amount of grafting is not desired however, because it changes the CNT sp^2 hybridization, and this negatively affects the CNT properties.[29]

WAXS

The WAXS spectrum for the crude powder is shown in Figure 10. The deconvolution of the profile into individual signals was done with GRAMS/386 software (Galactic Industries Corp., Woburn, MA). Deconvolution signals were allowed to be a mix of Gaussian and Lorentzian fits, as is common for these patterns.[49] This Lorentzian component is attributed to the distribution

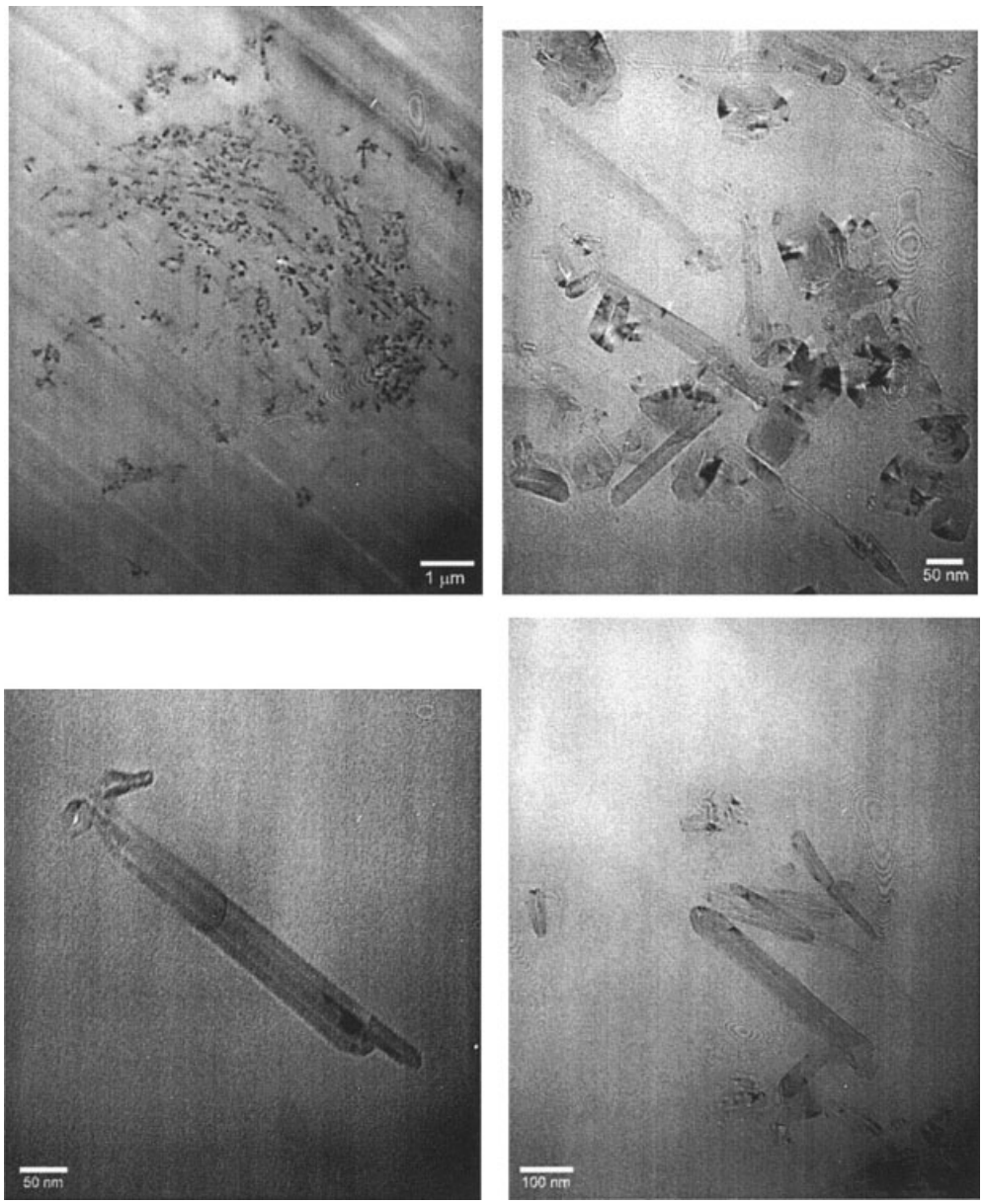

Figure 8 TEM micrographs of the 4.4 wt % composite sample (5 wt % crude powder in the original dispersion).

of interlayer spacing. The combination of Gaussian and Lorentzian signals resulted in the best agreement between deconvoluted and experimental profiles. The labels shown in the crude powder profile are the distances related to the scattering angle (θ) position of the maxima of the deconvoluted peaks. These distances were calculated with Bragg's law:[50]

$$\lambda = 2d \sin \theta \tag{2}$$

where λ is the X-ray wavelength and d is the characteristic spacing. The broad signal with a maximum at $2\theta = 23.6°$ ($d = 3.76$ Å) is the background scattering of the quartz tube and is unrelated to the scattering of the crude powder (MWNTs and graphitic particles/carbon soot). Two sharp signals can be seen at $2\theta = 26.25°$ and $2\theta = 27.85°$ ($d = 3.39$ Å and $d = 3.2$ Å, respectively). The first signal has been reported as the diffraction signature of the distance between walls in MWNTs ($d = 3.4$ Å).[10,51] The second signal at 3.2 Å is attributed to CNT–CNT alignment. Thess et al.[52] obtained a lattice constant and tube diameter of SWNT bundles from which a spacing of 3.2 Å can be calculated. Charlier et al.[53] calculated the most stable SWNT packing distance to be 3.14 Å, found in hexagonal packing. Girifalco et al.[54] calculated the equilibrium distance between infinitely long aligned SWNTs as a function of their diameter. Their calculations found a distance between NT walls for tubes of 24 nm of 3.13 Å. It can therefore be concluded that this signal is due to aligned MWNTs in the sample. The signal at

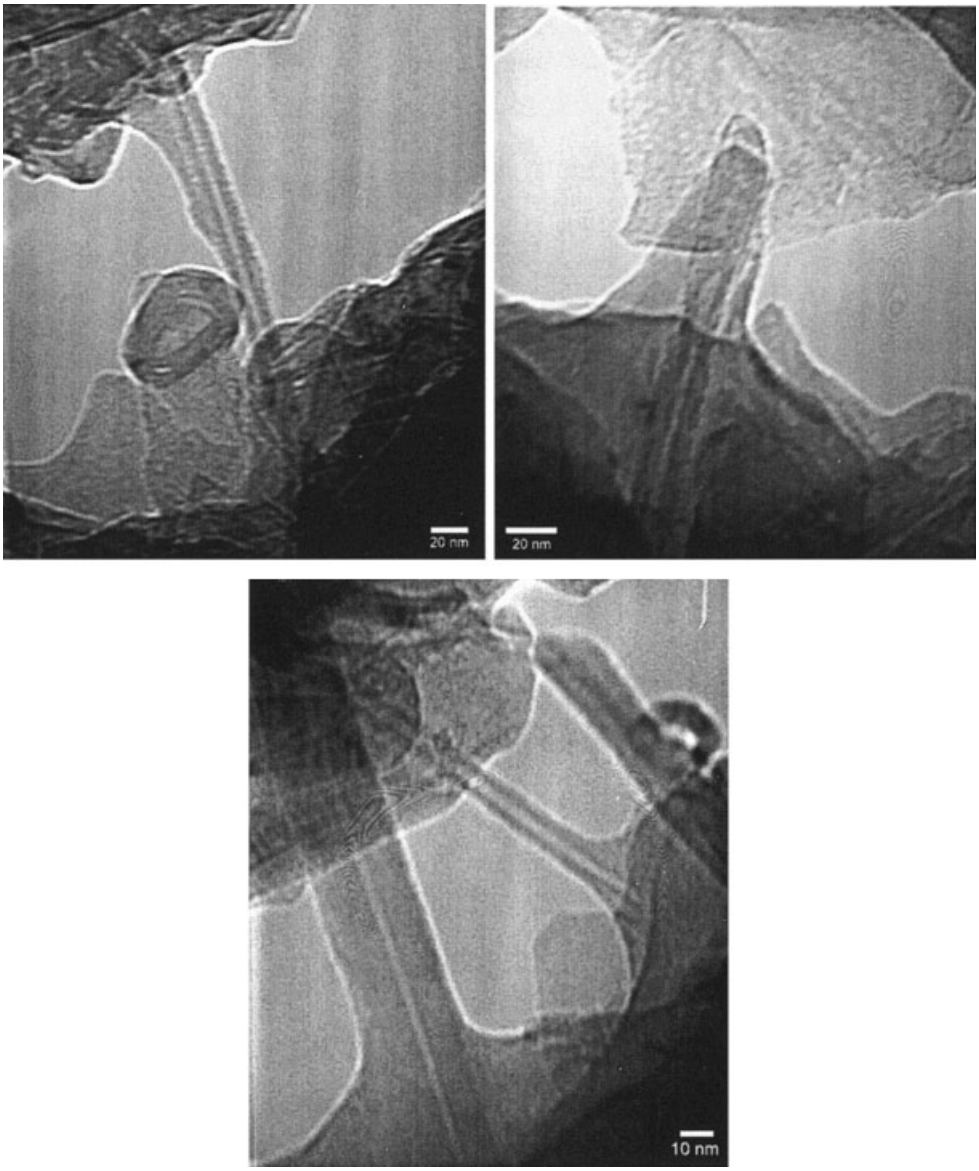

Figure 9 TEM micrographs of MWNTs sticking out of the polymer matrix at ruptured composite sections. The nanotubes are partially covered by the polymer. Because the thermosetting polymers cannot easily deform, sticking of the polymer matrix to the dispersed nanotubes is a sign of substantial interfacial strength potentially due to some grafting polymerization.

$2\theta = 43.4°$ ($d = 2.08$ Å) is attributed to the MWNT interwall spacing as well.[55] The two MWNT interwall signals discussed ($2\theta = 26.25°$ and $2\theta = 43.4°$) have been determined to be the reflections of the (002) and (004) graphitic planes, respectively.[55] Finally, the signals at lower angles ($2\theta = 4.23°$ and $2\theta = 0.78°$, or $d = 20.89$ Å and $d = 113.8$ Å) are due to low-angle scattering of amorphous carbon and graphitic particles.[56,57] The lowest angle signal has to be viewed with caution because it is too close to the limit of the detector. Duclaux et al.[56] performed a variety of WAXS experiments in the low-angle limit. A signal at 4.22° was assigned in this work to reflections of the (002) plane in amorphous carbon and graphitic articles. These particles have been shown to be present in the crude powder in large quantities.

Figure 10(b) shows the diffraction profiles of the pure polymer and composite samples. The profiles are shifted vertically for easier interpretation. The pure polymer sample shows the expected halo seen for all amorphous polymers. Two maxima in this amorphous halo can be seen at $2\theta = 21.56°$ and $2\theta = 8.48°$. With Bragg's law, these correspond to distances of 4.12 and 10.42 Å, respectively. The shortest distance of 4.12 Å can be attributed to the van der Waals contacts between carbon atoms of paraffin chains in random chain configurations[58] found in the triglyceride molecule of AESO (Fig. 1). The value found here is marginally lower than the generally reported distance range of 4.2–4.65 Å;[58] the lower values are signs of some molecular ordering such as crystallization. This range of values, however, was found to be valid for

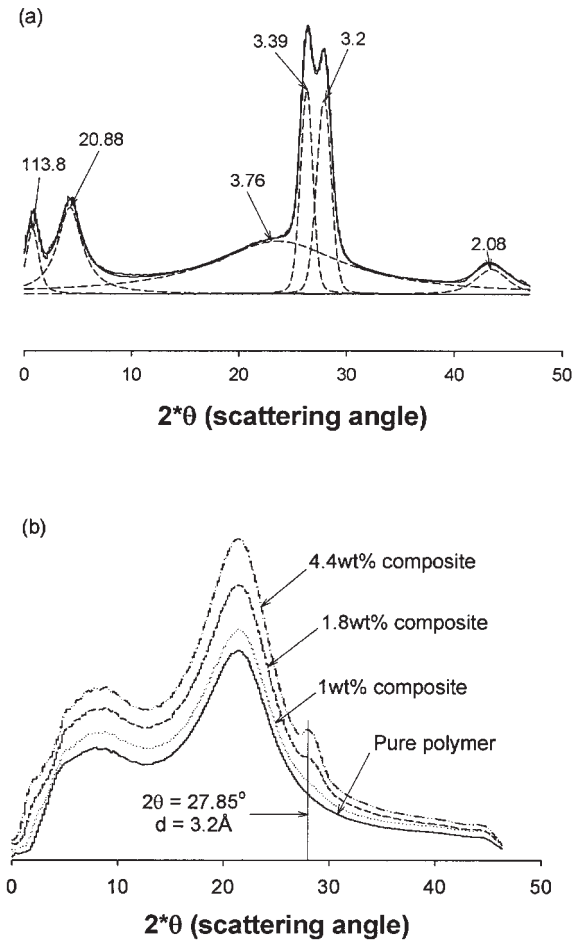

Figure 10 WAXS profiles versus 2θ. (a) The profile shows the signals from the crude powder with deconvoluted peaks. The labels refer to the distances (Å) related to θ by Bragg's law. (b) The diffraction profile shows the signals for the polymer and composite samples. These spectra have been offset vertically for easier interpretation.

aliphatic thermoplastic polymers. The incorporation of styrene and crosslinking result in a decrease in the free volume; this is apparent in the marked increase in density upon crosslinking and the higher density of polystyrene in comparison with that of aliphatic polymers.[59] This decrease results in an increase in the packing density and thus the lower value of 4.12 Å. The second, 10.42Å distance correlates with the length of the branches on the main chains.[58] If we consider the acrylate side groups on the AESO molecule, the number of carbon atoms can be correlated to a spacing distance of 10 Å, in good agreement with the experimental value. The deconvolution of the polymer diffraction profile could not be performed because it was too diffuse. The deconvolution results were too dependent on the choice of the amount of signals. This can be expected because the total profile is the sum of a large amount of small scattering signals due to the amorphous polymer matrix. The interwall MWNT peak at $2\theta = 26.25°$ ($d = 3.4$ Å) cannot be seen for any of the composite samples because of the amorphous halo of the polymer matrix. The WAXS results of the composite samples do show an increasing signal representing the 3.20Å distance with increasing MWNT content. It can be seen in the TEM micrographs that there were still a significant amount of aligned MWNTs in the composite samples, and this is consistent with these scattering results. It can also be expected that the amount of aligned MWNTs will increase with increased aggregation. With complete aggregation of the 1.8 wt % composite sample, it is possible to determine a dispersion efficiency (ε_d). This parameter measures the relative amount of MWNT alignment. The relative signal height at 3.2 Å, corrected for the amorphous halo interference, for the 1.8 wt % composite sample is used to define the maximum amount of alignment in the 1.8 wt % sample. Together with a 3.2Å signal height of zero for the pure polymer, it is possible to calculate the expected relative signal height for the 1 and 4.4 wt % composite samples with maximum alignment. ε_d is then defined as the relative difference between this maximum alignment height and the actually measured, corrected signal height:

$$\varepsilon_d = 1 - \frac{\left[\dfrac{A_{\text{corr}}(3.2\text{Å})}{A(4.12\text{Å})}\right]}{\left[\dfrac{A_{\text{corr}}^{1.8\text{wt\%}}(3.2\text{Å})}{A^{1.8\text{wt\%}}(4.12\text{Å})}\right] \times \dfrac{\text{wt\%}}{1.8\ \text{wt\%}}} \qquad (3)$$

where $A(i)$ is the signal height at distance i, with the subscript corr denoting the signal height corrected for the polymer halo interference and the superscript 1.8 wt % denoting the signal for the 1.8 wt % composite sample. The term $^{\text{wt \%}}/_{1.8\ \text{wt \%}}$ corrects the signal height for maximum alignment for the 1.8 wt % composite sample to the value for the sample under investigation. The 3.2Å signal also includes dispersed aligned nanotube signals. This is acceptable because the alignment of dispersed CNTs will also reduce the reinforcement capability of CNTs. The calculated ε_d values for the 1 and 4.4 wt % composite samples are 70.7 and 10%, respectively. Taking the purity of the crude powder to be 40%, we have found the amount of effectively dispersed MWNTs in the composites to be 0.283 and 0.174 wt % for the 1 and 4.4 wt % composite samples, respectively. These values can only be expected to be estimates of the amount of dispersed MWNTs. Nevertheless, they are consistent with E' measured with DMA.

Property analysis

Several reinforcement models can be used to describe the reinforcing behavior of CNTs. The most common models used are the upper bound rule of mixtures and the Halpin–Tsai equation.[60–62] The Halpin–Tsai equa-

tion for composites reinforced with randomly oriented CNTs is given by[63–65]

$$E_C = \left[\frac{3}{8}\frac{1 + 2a_{CNT}\eta_L\phi_{CNT}}{1 - \eta_L\phi_{CNT}} + \frac{5}{8}\frac{1 + 2\eta_T\phi_{CNT}}{1 - \eta_T\phi_{CNT}}\right]E_M$$

$$\eta_L = \frac{\left(\frac{E_{CNT}}{E_M}\right) - 1}{\left(\frac{E_{CNT}}{E_M}\right) + 2a_{CNT}} \qquad \eta_T = \frac{\left(\frac{E_{CNT}}{E_M}\right) - 1}{\left(\frac{E_{CNT}}{E_M}\right) + 2} \tag{4}$$

where $a_{CNT} = l_{CNT}/d_{CNT}$ is the aspect ratio, l_{CNT} and d_{CNT} being the length and diameter of the nanotubes, respectively; ϕ_{CNT} is the CNT volume fraction; and E_{CNT}, E_M, and E_C are the moduli of the CNTs, matrix, and composite, respectively. Thostenson and Chou[62] suggested a correction to the CNT modulus due to its hollow core and based on micromechanics:

$$E_{CNT,eff} = \frac{4t}{d}E_{CNT} \tag{5}$$

where t is the nanotube wall thickness and d is the diameter. Equation (5) is only valid for $t/d < 0.25$, and the correlation of the tube wall thickness with the diameter[62] shows that this constraint is only valid for CNTs with diameters less than 13 nm. Because the average diameter of the MWNTs used in this work is 24 nm, this correction is not applicable. The success of the Halpin–Tsai model and the rule of mixtures to describe the reinforcement of composites with randomly oriented CNTs is quite varied. The fitting of the Halpin–Tsai model to experimental data, with the aspect ratio as a variable, commonly results in large overpredictions of the aspect ratio. The fitted CNT lengths have been found to be several orders of magnitude larger than what is determined by electron microscopy.[60] The rule of mixtures has a more varied record, with the fitted CNT modulus being both overpredicted and underpredicted from reported values.[60] Cadek et al.[60] recently developed a new model based on the CNT surface area:

$$E_C = \left(\frac{4k}{d}\phi_{CNT} + 1\right)E_M \tag{6}$$

where k is a parameter describing the strength of the CNT–polymer interface. Other parameters are consistent with previous definitions. This model is quite interesting, in that it does not include the CNT modulus. The reasoning is the relative weakness of the CNT–matrix interface, compared with the CNT modulus, such that the interface is expected to fail before the CNT does. The full reinforcement potential of CNTs can thus not be attained. Equation (6) is successful in describing the tensile modulus for a wide variety of different CNTs and CNT weight fractions in a poly(vinyl alcohol) (PVA) matrix.[60] A universal k parameter was found for these composites of 468 ± 114 nm. This would suggest that small-diameter CNTs (resulting in larger surface area per unit of volume) would be the most efficient reinforcements.

Figure 11 shows the experimental results in comparison with different reinforcement models: the upper bound rule of mixtures

$$E_C = \phi_M E_M + \phi_F E_F \tag{7}$$

the lower bound rule of mixtures

$$\frac{1}{E_C} = \frac{\phi_M}{E_M} + \frac{\phi_F}{E_F} \tag{8}$$

with ϕ_M the matrix volume fraction, the Halpin–Tsai model [eq. (4) with $a_{CNT} = 33.33$], and Cadek et al.'s model [eq. (6) with $k = 468$ nm]. The MWNT modulus was taken to be 1 TPa.[61] The polymer and MWNT density were taken to be 1.07 and 1.9 g/cm^3, respectively. The MWNT density was reported by Thostenson and Chou[62] to be lower than the graphite density of 2.2 g/cm^3. The weight fraction of MWNTs used in the calculation was obtained by the multiplication of the TGA-determined crude powder amount with the MWNT purity, taken to be 40%. The experimental data fall within the boundaries of the two rules of mixtures, as could be expected. The Halpin–Tsai model underpredicts the experimental results, and this is expected because of the need for higher than actual aspect ratios to fit experimental results.[60] Cadek et al.'s model underpredicts the experimental result for 1 wt %. Because the maximum MWNT content in the crude powder has been used for the volume fraction calculations, this can only be due to a higher interfacial strength between the polymer and dispersed MWNTs. The k value used in the model predictions was experimentally determined for thermoplastic PVA composites.[60] The interface is largely dependent on the van der Waals interactions between the polymer and MWNT.[66,67] The considerable increase for the 1 wt % sample suggests a strong polymer–MWNT interface, possible due to some grafting during polymerization. Active radicals can react with the sp^2 hybridized structure of the CNTs and form covalent bonds. This has been shown to occur during the free-radical bulk polymerization of methyl methacrylate.[68,69] These results clearly show an enormous potential for MWNT–AESO/styrene composites.

CONCLUSIONS

The work presented here on CNTs allows us to draw some very important conclusions with respect to

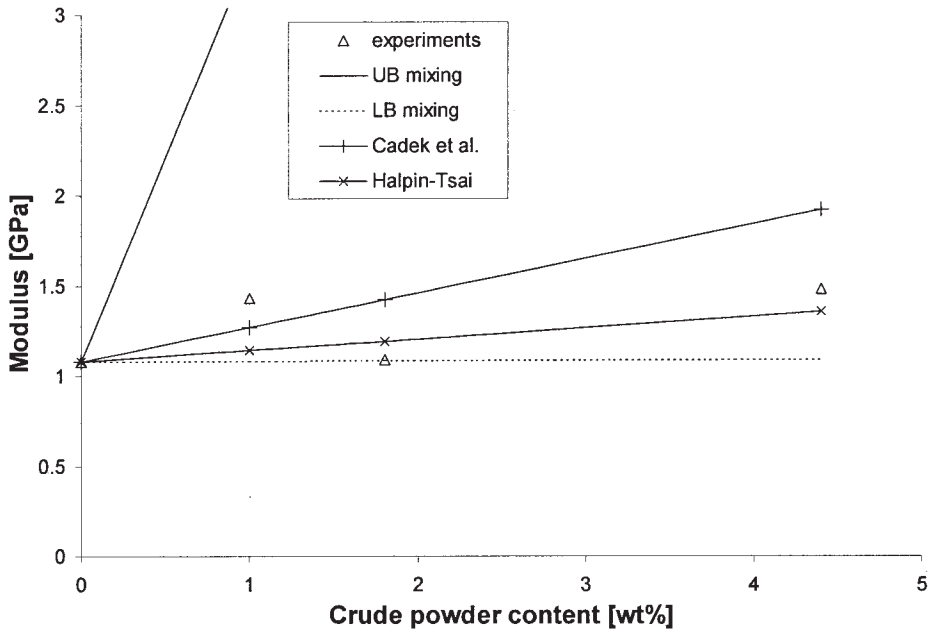

Figure 11 Comparison of the experimental E' values at 35°C with the models described in the text. UB mixing is the upper bound rule of mixtures [eq. (5)], LB mixing is the lower bound rule of mixtures [eq. (6)], the Halpin–Tsai model is described by eq. (2), and Cadek et al.'s model was calculated from eq. (4) with $k = 468$ nm.

MWNT/unsaturated thermoset composites and the AESO/styrene system in particular. The ability of AESO to disperse MWNTs with simple mixing is a further confirmation of the earlier reported dispersing capacity of AESO with respect to SWNTs. The stirring time needs to be increased with increasing MWNT/carbon soot content, as can be expected. The subsequent polymerization of these stable dispersions, however, leads to aggregation of the carbon soot, apparently dragging MWNTs into the aggregates during this process. The result is a marked decrease of free and thus reinforcing MWNTs in the composite sample with growing carbon soot content. TEM, WAXS, and DMA results agree with this process. Additionally, TEM shows very good adhesion between the resin matrix and the reinforcing MWNTs, potentially due to some limited grafting. Underprediction of the experimental data by the generally used descriptive models for these composites also points to a strong interface between MWNTs and the resin matrix. One can thus conclude that the use of crude powder, containing MWNTs and carbon soot, as a cheaper source of MWNTs as reinforcements of thermosetting polymers is only viable at small volume fractions. Additionally, the AESO/styrene resin system looks very promising as matrix material for CNT composites, and work is currently in progress to investigate the MWNT–AESO interactions during and after polymerization with pure MWNTs.

The authors thank Martin Cadek (Trinity College Dublin) for supplying the multiwall carbon nanotube crude powder in amounts that allowed them to make the larger composite samples. One of the authors (W.T.) also thanks Jonathan Coleman (Trinity College Dublin) and Marc in het Panhuis (University of Texas at Dallas) for the valuable interactions.

References

1. Troianni, H. E.; Miki-Yoshida, M.; Camacho-Bragado, G. A.; Marques, M. A. L.; Rubio, A.; Ascencio, J. A.; Jose-Yacaman, M. Nano Lett 2003, 3, 751.
2. Thostenson, E. T.; Ren, Z.; Chou, T.-W. Compos Sci Technol 2001, 61, 1899.
3. Saito, R.; Kataura, H. Top Appl Phys 2001, 80, 213.
4. Wan, X.; Dong, J.; Xing, D. Y. Phys Rev B 1998, 58, 6756.
5. Tang, Z. K.; Zhang, L. Y.; Wang, N.; Zhang, X. X.; Wang, J. N.; Li, G. D.; Li, Z. M.; Wen, G. H.; Chan, C. T.; Sheng, P. Synth Met 2003, 133, 689.
6. Ouyang, M.; Huang, J.-L.; Lieber, C. M. Acc Chem Res 2002, 35, 1018.
7. Darkrim, F. L.; Malbrunot, P.; Tartaglia, G. P. Int J Hydrogen Energy 2002, 27, 193.
8. Wong, E. W.; Sheehan, P. E.; Lieber, C. M. Science 1997, 277, 1971.
9. Treacy, M. M.; Ebbesen, T. W.; Gibson, C. M. Nature 1996, 381, 678.
10. Hilding, J.; Grulke, E. A.; Zhang, Z. G.; Lockwood, F. J Dispersion Sci Technol 2003, 24, 1.
11. Ausman, K. D.; Piner, R.; Lourie, O.; Ruoff, R. S.; Korobov, M. J Phys Chem B 2000, 104, 8911.
12. Dai, H. Acc Chem Res 2002, 35, 1035.
13. Jiang, L.; Gao, L.; Sun, J. J Colloid Interface Sci 2003, 260, 89.
14. Gong, X.; Baskaran, S.; Voise, R. D.; Young, J. S. Chem Mater 2000, 12, 1049.
15. McCarthy, B.; Coleman, J. N.; Czerw, R.; Dalton, A. B.; in het Panhuis, M.; Maiti, A.; Drury, A.; Byrne, H. J.; Carroll, D. L.; Blau, W. J. J Phys Chem B 2002, 106, 2210.
16. in het Panhuis, M.; Maiti, A.; Dalton, A. B.; van den Noort, A.; Coleman, J. N.; McCarthy, B.; Blau, W. J. J Phys Chem B 2003, 127, 478.

17. Dalton, A. B.; Stephan, C.; Coleman, J. N.; McCarthy, B.; Ajayan, P. M.; Lefrant, S.; Bernier, P.; Blau, W. J.; Byrne, H. J. J Phys Chem B 2000, 104, 10012.
18. Bandyopadhyaya, R.; Nativ-Roth, E.; Regev, O.; Yerushalmi-Rozen, R. Nano Lett 2002, 2, 25.
19. Chen, J.; Dyer, M. J.; Yu, M.-F. J Am Chem Soc 2001, 123, 6201.
20. Chambers, G.; Carroll, C.; Farrell, G. F.; Dalton, A. B.; McNamara, M.; Cummins, E.; in het Panhuis, M.; Byrne, H. J. Nano Lett 2003, 3, 843.
21. in het Panhuis, M.; Salvador-Morales, C.; Franklin, E.; Chambers, G.; Fonseca, A.; Nagy, J. B.; Blau, W. J.; Minett, A. I. J Nanosci Nanotechnol 2003, 3, 209.
22. Dieckmann, G. R.; Dalton, A. B.; Johnson, P. A.; Razal, J.; Chen, J.; Giordano, G. M.; Muñoz, E.; Musselman, I. H.; Baughman, R. H.; Draper, R. K. J Am Chem Soc 2003, 125, 1770.
23. Georgakilas, V.; Tagmatarchis, N.; Pantarotto, D.; Bianco, A.; Briand, J. P.; Prato, M. Chem Commun 2002, 24, 3050.
24. Banerjee, S.; Wong, S. S. J Phys Chem B 2002, 106, 12144.
25. Whitsitt, E. A.; Barron, A. R. Nano Lett 2003, 3, 775.
26. Lee, Y. S.; Cho, T. H.; Lee, B. K.; Rho, J. S.; An, K. H.; Lee, Y. H. J Fluorine Chem 2003, 120, 99.
27. Khabashesku, V. N.; Billups, W. E.; Margrave, J. L. Acc Chem Res 2002, 35, 1087.
28. Boul, P. J.; Mickelson, E. T.; Huffman, C. B.; Ericson, L. M.; Chiang, I. W.; Smith, K. A.; Colbert, D. T.; Hauge, R. H.; Margrave, J. L.; Smalley, R. E. Chem Phys Lett 1999, 310, 367.
29. Garg, A.; Sinnott, S. B. Chem Phys Lett 1998, 295, 273.
30. Richard, C.; Balavoine, F.; Schultz, P.; Ebbesen, T. W.; Mioskowski, C. Science 2003, 300, 775.
31. Khot, S. N.; LaScala, J. J.; Can, E.; Morye, S. S.; Williams, G. I.; Palmese, G. R.; Kusefoglu, S. H.; Wool, R. P. J Appl Polym Sci 2001, 82, 703.
32. Thielemans, W.; Can, E.; Morye, S. S.; Wool, R. P. J Appl Polym Sci 2002, 83, 323.
33. O'Donnel, A.; Dweib, M. A.; Wool, R. P. Compos Sci Technol 2004, 64, 1135.
34. Thielemans, W.; Wool, R. P. Compos A 2004, 35, 327.
35. Wool, R. P.; Khot, S. N.; LaScala, J. J.; Bunker, S. P.; Thielemans, W.; Can, E.; Morye, S. S.; Williams, G. I. In Advancing Sustainability through Green Chemistry; Lankey, R. L.; Anastas, P. T., Eds.; ACS Symposium Series 823; American Chemical Society: Washington, DC, 2002; p 177.
36. Wool, R. P.; Khot, S. N.; LaScala, J. J.; Bunker, S. P.; Thielemans, W.; Can, E.; Morye, S. S.; Williams, G. I. In Advancing Sustainability through Green Chemistry; Lankey, R. L.; Anastas, P. T., Eds.; ACS Symposium Series 823; American Chemical Society: Washington, DC, 2002; p 205.
37. Liu, K. Soybeans: Chemistry, Technology, and Utilization; Chapman & Hall: New York, 1997.
38. Panhuis, M. I. H.; Thielemans, W.; Minett, A. I.; Leahy, R.; Blau, W. J.; Le Foulgoc, B.; Wool, R. P. Int J Nanosci 2003, 2, 185.
39. Sandler, J.; Schaffer, M. S. P.; Prasse, T.; Bauhofer, W.; Schulte, K.; Windle, A. H. Polymer 1999, 40, 5967.
40. Cadek, M.; Murphy, R.; McCarthy, B.; Drury, A.; Lahr, B.; Barklie, R. C.; Panhuis, M.; Coleman, J. N.; Blau, W. J. Carbon 2002, 40, 923.
41. Kandola, B. K.; Horrocks, A. R.; Myler, P.; Blair, D. ACS Symposium Series 797; American Chemical Society: Washington, DC, 2001; p 344.
42. Das, A. N.; Baijal, S. K. J Appl Polym Sci 1982, 27, 211.
43. Coleman, J. N.; O'Brien, D. F.; Dalton, A. B.; McCarthy, B.; Lahr, B.; Drury, A.; Barklie, R. C.; Blau, W. J. Chem Commun 2000, 2001.
44. Perminov, V. P.; Modyanova, A. G.; Ryabkov, Y. I.; Sevbo, O. A.; Gailyunas, I. A.; Kuchin, A. V. Russ J Appl Chem 2002, 75, 636.
45. Witort, I.; Tadeusz, S.; Wladyslaw, C.; Bronislaw, J. Polymery 1976, 21, 155.
46. Narkis, M.; Rafail, I.; Victor, G.; Tzur, A.; Tchoudakov, R.; Siegmann, A. J Appl Polym Sci 2000, 76, 1165.
47. Narkis, M.; Zilberman, M.; Siegman, A. Polym Adv Technol 1997, 8, 525.
48. Sweitzer, C. W.; Lyon, F.; Grabowski, T. S. Ind Eng Chem 1955, 47, 2380.
49. Reznik, D.; Olk, C. H.; Neumann, D. A.; Copley, J. R. D. Phys Rev B 1995, 52, 116.
50. Baltá-Calleja, F. J.; Vonk, C. G. X-Ray Scattering of Synthetic Polymers; Polymer Science Library 8; Elsevier: New York, 1989.
51. Saito, Y.; Yoshikawa, T.; Bandow, S.; Tomita, M.; Hayashi, T. Phys Rev B 1993, 48, 1907.
52. Thess, A.; Lee, R.; Nikolaev, P.; Dai, H.; Petit, P.; Robert, J.; Xu, C.; Lee, Y. H.; Kim, S. G.; Rinzler, A. G.; Colbert, D. T.; Scuseria, G. E.; Tomanek, D.; Fischer, J. E.; Smalley, R. E. Science 1996, 273, 483.
53. Charlier, J.-C.; Gonze, X.; Michenaud, J.-P. Europhys Lett 1995, 29, 43.
54. Girifalco, L. A.; Hodak, M.; Lee, R. S. Phys Rev B 2000, 62, 13104.
55. Dore, J.; Burian, A.; Tomita, S. Acta Phys Pol A 2000, 98, 495.
56. Duclaux, L.; Salvetat, J. P.; Lauginie, P.; Cacciaguera, T.; Faugere, A. M.; Goze-Bac, C.; Bernier, P. J Phys Chem Solids 2003, 64, 571.
57. Maniwa, Y.; Fujiwara, R.; Kira, H.; Tou, H.; Nishibori, E.; Takata, M.; Sakata, M.; Fujiwara, A.; Zhao, X.; Iijima, S.; Ando, Y. Phys Rev B 2001, 64, 073105-1.
58. Jones, A. T. Makromol Chem 1964, 71, 1.
59. Van Krevelen, D. W. Properties of Polymers: Their Correlation with Chemical Structure; Their Numerical Estimation and Prediction from Additive Group Contributions; Elsevier: Amsterdam, 1997.
60. Cadek, M.; Coleman, J. N.; Ryan, K. P.; Nicolosi, V.; Bister, G.; Fonseca, A.; Nagy, J. B.; Szostak, K.; Beguin, F.; Blau, W. J. Nano Lett 2004, 4, 353.
61. Qian, D.; Dickey, E. C.; Andrews, R.; Rantell, T. Appl Phys Lett 2000, 76, 2868.
62. Thostenson, E. T.; Chou, T.-W. J Phys D: Appl Phys 2003, 36, 573.
63. Halpin, J. C.; Kardos, J. L. Polym Eng Sci 1976, 16, 344.
64. Talreja, R.; Manson, J.-A. E. In Comprehensive Composite Materials; Kelly, A.; Zweben, C. H., Eds.; Elsevier: New York, 2000; Vol. 2, p 307.
65. Cadek, M.; Coleman, J. N.; Barron, V.; Hedicke, K.; Blau, W. Appl Phys Lett 2002, 81, 5123.
66. Li, C.; Chou, T.-W. J Nanosci Nanotechnol 2003, 3, 1.
67. Li, C.; Chou, T.-W. Compos Sci Technol 2003, 63, 1517.
68. Jia, Z.; Wang, Z.; Xu, C.; Liang, J.; Wei, B.; Wu, D.; Zhu, S. Mater Sci Eng A 1999, 271, 395.
69. Park, S. J.; Cho, M. S.; Lim, S. T.; Choi, H. J.; Jhon, M. S. Macromol Rapid Commun 2003, 24, 1070.